Multiple scattering of slow ions in a partially degenerate electron fluid

Romain Popoff,* Gilles Maynard, and Claude Deutsch
Laboratoire de Physique des Gaz et des Plasmas, UMR 8578, Université Paris-Sud XI, Orsay 91400, France
(Received 13 October 2008; revised manuscript received 2 June 2009; published 28 October 2009)

We extend former investigation to a partially degenerate electron fluid at any temperature of multiple slow ion scattering at $T=0$. We implement an analytic and mean-field interpolation of the target electron dielectric function between $T=0$ (Lindhard) and $T\to\infty$ (Fried-Conte). A specific attention is given to multiple scattering of proton projectiles in the keV energy range, stopped in a hot-electron plasma at solid density.

DOI: 10.1103/PhysRevE.80.046408 PACS number(s): 52.25.Mq, 31.15.bt, 52.58.Ei

I. INTRODUCTION

The purpose of the present paper is to contribute to the investigation of the basic interaction physics involved in the recently reoriented U.S. heavy-ion program [1–3] and now mostly devoted to the production of the so-called warm dense matter (WMD), i.e., plasmas at ordinary matter density with a few eV temperature. Toward this goal, it is proposed [2,3] to accelerate linearly intense ion beams impacting thin foils.

The given ion-target interaction is also supposed to take place at moderate or low projectile velocity ($\sim$0.03–3 MeV/a) [3] near Bragg peak, thus featuring a maximum, as well as mostly homogenous, energy deposition in a thin foil. We thus focus the attention on the very low velocity regime for the ion projectile with an oriented velocity $v_p \leq v_{\mathrm{the}}$, with v_{the} denoting the target electron thermal velocity. Relevant ion stopping issues for relatively light projectile ($Z\leq 24$) have already been alluded to [1,3]. In this case, the actual projectile penetration depth [4] should be routine evaluated through an estimate of multiscattering (MS) on target ions. Moreover, recent studies dedicated to the stopping of intense relativistic and PetaWatt (PW) laser-produced electron beams have also unraveled a non-negligible contribution to MS due to the target electrons [5]. With these promises in mind, we are thus lead to extend at any target temperature T a recent MS treatment for low velocity ion projectiles in a fully degenerate electron jellium at $T=0$ essentially due to Archubi and Arista [6]. The WDM parameters range puts a strong emphasis on the partial degeneracy of target electrons with $T\geq 10$ eV.

Toward this goal, we heavily rely on the mean-field and interpolated dielectric function [7–9] $\varepsilon(q,\omega)$ between the $T=0$ (Lindhard) [10] and the high-temperature (Fried-Conte) [11] corresponding limits, as worked out by the Orsay group and others [7–9,12]. Similar efforts have also been focused on low velocity ion slowing down in partially degenerate electron fluid through a nonlinear treatment of the T dependence [13].

The sequel is structured as follows. In Sec. II, we stress the usefulness of pseudoanalytic expressions [8] for the RPA $\varepsilon(q,\omega)$ at any T out of former exact interpolations [7]. From them, in Sec. III, single-scattering features are derived through the probability function $G(q_\perp)$ in terms of transverse momentum. In Sec. IV, we turn to multiple scattering and focus our attention on the half angle at half maximum $\alpha_{1/2}$ through a parameter investigation in terms of electron target temperature T, thickness X, and density number n_e, as well as ion projectile velocity v_p. A numerical and efficient extension of the Bethe ansatz is in Sec. V. Summaries are briefly outlined in Sec. VI.

II. $\varepsilon(Q,\omega)$ AT ANY TEMPERATURE T

Among the several available presentations [7–9] of the interpolated random-phase approximation (RPA) dielectric function $\varepsilon(q,\omega)$, the one advocated by Arista and Brandt [8] seems especially suited to the present analysis. In view of the low ion velocity v_p advocated here, we may safely restrict to a quasistatic approximation ($v_p \leq v_{\mathrm{the}}$, where v_{the} includes a Pauli repulsion contribution for $T\leq T_F$, T_F being Fermi temperature) such that $\omega\to 0$. Then, explicating the complex $\varepsilon(q,\omega)$ as

$$\varepsilon(q,\omega) = \varepsilon_r(q,\omega) + i\varepsilon_i(q,\omega), \tag{1}$$

we can use the approximation $|\varepsilon_r(q,\omega)| \ll |\varepsilon_i(q,\omega)|$ to validate the so-called stopping function under the form

$$\mathrm{Im}\left[-\frac{1}{\varepsilon(q,\omega}\right] = \frac{\varepsilon_i(q,\omega)}{|\varepsilon(q,\omega)|^2} \approx \frac{\varepsilon_i(q,\omega)}{\varepsilon_r^2(q,\omega)}, \tag{2}$$

yielding the spectrum of plasma excitations in terms of momentum transfer $\hbar q$ and energy $\hbar\omega$, so in the $\omega\to 0$ limit and with Table II of Ref. [8], we get

$$S(q,\omega) \cong \mathrm{Im}\left[-\frac{1}{\varepsilon(q,\omega}\right] \cong \frac{2m^2e^2q\omega}{\hbar^3(q^2+q_s^2)^2}\cdot\frac{1}{1+\exp\left(\frac{\hbar^2q^2}{8m_eT}-\eta\right)}, \tag{3}$$

with $\eta=\beta\mu$ pictured on Fig. 1, where $\beta=(k_BT)^{-1}$ and μ the chemical potential of the partially degenerate electron fluid (PDEF). q_s^2 (see Fig. 2) is obtained from η through

$$q_s^2 = \frac{1}{2}q_{\mathrm{TF}}^2\theta^{1/2}F_{-1/2}(\eta), \tag{4}$$

with q_{TF} the Thomas-Fermi screening parameter and

*romain.popoff@u-psud.fr

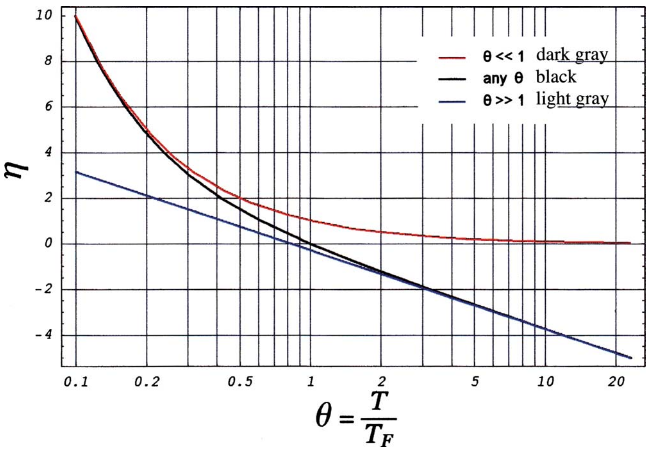

FIG. 1. (Color online) $\eta(=\frac{\mu}{k_B T})$ in terms of $\theta=\frac{T}{T_F}$.

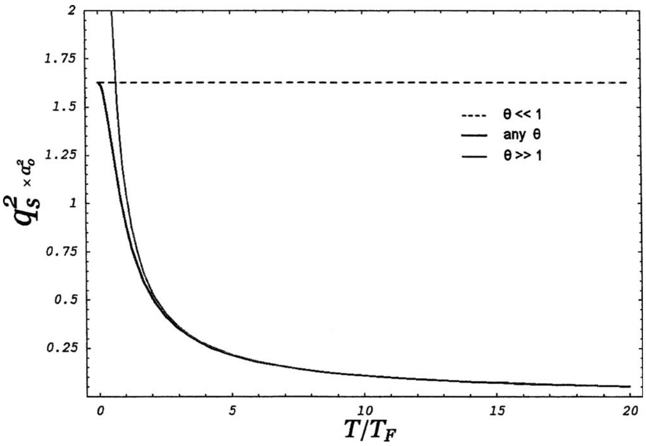

FIG. 2. q_s^2 (a.u.) in terms of $\theta=\frac{T}{T_F}$.

$$F_\nu(\eta)=\int_0^\infty \frac{x^\nu}{1+e^{x-\eta}}dx$$

the Fermi function. It should be appreciated that we deleted the usual Bose factor $N(\omega)$ in reducing Eq. (3) to the energy-loss function because $N(\omega)$ gets finally cancelled in the (q,ω) quadrature featuring the stopping-power expression [8].

(i) The extreme limits of η with respect to temperature

$$\eta \approx \begin{cases} \frac{1}{\theta}(\theta \ll 1) \\ \ln\left(\frac{4}{3\sqrt{\pi}\theta^{3/2}}\right) \end{cases} \tag{5}$$

are given on Fig. 1 altogether with the exact interpolating black curve η valid at any T (or equivalently θ).

(ii) q_s^2 advocate the two $\theta=\frac{T}{T_F}$ limits

$$q_s^2 \approx \begin{cases} \frac{q_{\mathrm{TF}}^2}{\sqrt{1+\frac{9\theta^2}{4}}}(\theta<1) \\ \frac{1/\lambda_D^2}{\sqrt{1+\frac{4}{9\theta^2}}}(\theta>1) \end{cases}$$

and corresponding limit

$$q_s^2 \approx \begin{cases} \lim_{\theta\ll 1} q_s = q_{\mathrm{TF}} = \sqrt{3}\frac{\omega_p}{v_F} \\ \lim_{\theta\gg 1} q_s = \frac{1}{\lambda_D} \end{cases}$$

in terms of PDEF frequency ω_p, $v_F=\hbar q_F/m_e$ the Fermi velocity with Fermi wave number $q_F=(3\pi^2 n_e)^{1/3}$, and λ_D the classical Debye screening length valid for $\theta€\gg 1$. These expressions altogether with the q_s^2 valid for all T are displayed on Fig. 2.

Then we can express the right-hand side of Eq. (3) in the two extreme limits by

(1) $\theta \ll 1$. Here, altogether with the q_s^2 valid for all T,

$$S(q,\omega) \cong \frac{2m^2e^2q\omega}{\hbar^3(q^2+q_{\mathrm{TF}}^2)^2}, \quad \text{for } q \le 2q_F,$$

$$S(q,\omega)=0, \quad \text{for } q>2q_F. \tag{6}$$

(2) $\theta \gg 1$. Here,

$$S(q,\omega) \cong \frac{n_e^2 m^2 e^2 q\omega}{(q^2+1/\lambda_D^2)^2}\left(\frac{2\pi}{m_e k_B T}\right)^{3/2}\exp\left(-\frac{\hbar^2q^2}{8m_e k_B T}\right). \tag{7}$$

Equation (6) corresponds to absorption of small amounts of energy $\hbar\omega \ll T_F$ by a degenerate electron gas. Owing to the exclusion principle, only those electrons close to the Fermi surface can participate. Thus, the momentum transfer $\hbar q$ can never be larger than $2q_F$.

This restriction is relaxed for high temperatures as shown by Eq. (7), where excitations with small ω but large q values occur—they involve electrons in the tail of the Maxwell-Boltzmann distribution and thus contribute with exponentially decaying probability. Yet, this is a characteristic quantum effect, as indicated clearly by the factor $\exp(-\hbar^2q^2/8m_e k_B T)$ which replaces the analogous factor $\exp(m\omega^2/2k_B T q^2)$ arising in classical theories.

III. SINGLE SCATTERING

Adapting the $T=0$ formalism (cf. [14,6]) for the ion projectile scattering probability expressed as

$$\frac{d^4P}{d^3q\,d\omega}=\frac{|F(q)|_2}{\pi^2q^2}\mathrm{Im}\left[\frac{-1}{\varepsilon(q,\omega}\right]\delta(\hbar\omega-\hbar\vec{q}\cdot\vec{v}_p), \tag{8}$$

with a pointlike projectile form factor $F(q)=Ze$, Z being the ion charge, and using the splitting $d^3q=d^2q_\perp\, dq_\parallel$ relative to initial beam velocity v_p, we get

$$\frac{d^2P}{d^2q_\perp}=\int \frac{d^3P}{d^3q}dq_\parallel$$

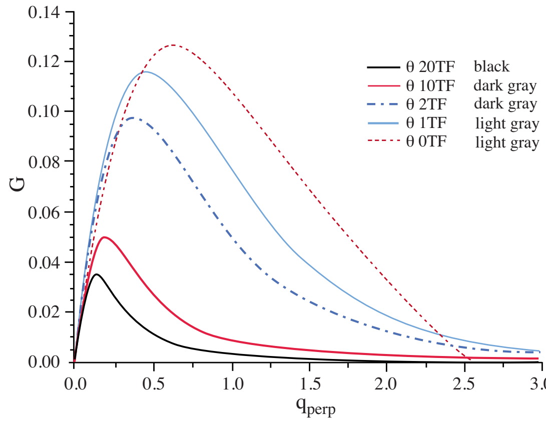

FIG. 3. (Color online) Probability distribution $G_{\forall T(q\perp)}$ at any temperature T contrasted to its FEG counterpart ($T=0$). $q_\perp$ in a_0^{-1} and $r_s=1.5$.

$$=\frac{1}{\hbar\pi^2}\int\frac{dq_\parallel}{q_\perp^2+q_\parallel^2}|F(q)|^2\mathrm{Im}\left[\frac{-1}{\varepsilon(q,\omega}\right]_{|\omega=q_\parallel v_p},\qquad(9)$$

expressing the probability of ion projectile differential scattering, yielding its angular deflections in single-scattering events through inclusion of the target electrons collective screening properties. Putting Eq. (3) into the above equation (9) yields

$$\frac{dP}{dq_\perp}=v_pG_{\forall T}(q_\perp),$$

where

$$G_{\forall T}(q_\perp)=\frac{4Z^2e^4m_e^2}{\hbar^4\pi}q_\perp\int_{q_\perp}^{\infty}\frac{1}{(q^2+q_s^2)^2}\frac{1}{1+\exp\left(\dfrac{\hbar^2}{8m_eT}q^2-\eta\right)}dq\qquad(10)$$

denotes the v_p-independent probability function. Equation (10) thus extends at any T value a former $T=0$ expression [6] derived within the framework of the so-called free-electron-gas (FEG) model.

Figure 3 depicts a typical $G_{\forall T}(q_\perp)$ scattering function contrasted to its $T=0$ (FEG) homologous for a typical target density $r_s=1.5$, where $4\pi r_s^3/3=1/n_e=4.8\times10^{23}$ cm^{-3}, for a proton projectile ($Z=1$). The function $G(q_\perp)$ at $T=0$ always features an upper bound for $G_{\forall T}(q_\perp)$. The latter slightly decreases with increasing T at fixed n_e, while its range steadily extends to higher $q_\perp$ values. Equation (10) is also contrasted to its high-temperature Fried-Conte limit [cf. Eq. (7)] on Fig. 3 featuring the lowest black curve.

Focusing attention on the strongly degenerate range $\theta\leq1$, one obtains corresponding G curves on Fig. 4, while extending $q_\perp$ to the θ values displayed on Fig. 3 yields the more complete G patterns featured on Fig. 5. Then, full degeneracy ($\theta=0$) is signaled by a vertical line.

IV. MULTIPLE SCATTERING

A. General

From the density probability function [Eq. (10)], we can access the differential cross section for ion multiple scattering in a PDEF. At a given transverse momentum transfer $\hbar q_\perp$, this quantity writes as

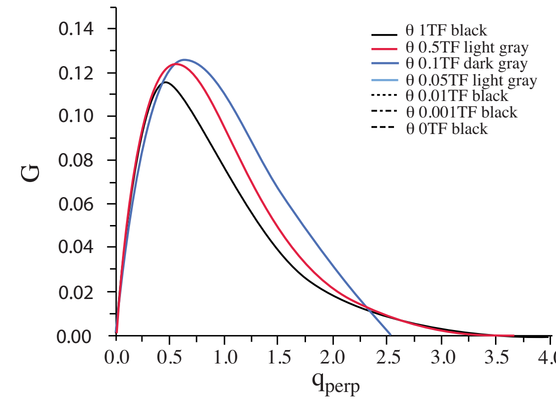

FIG. 4. (Color online) Same caption as Fig. 3 for $\theta\leq1$.

$$d\sigma=\frac{1}{n_ev_p}dP=\frac{1}{n_e}G_{\forall T}(q_\perp),\qquad(11)$$

with angular ion deflection ψ taken in the small-angle approximation $\hbar q_\perp=M_pv_p\psi$, with the ion projectile mass M_p.

Following the Sigmund-Winterbon procedure [6,15], we then turn to the convolution of the multiple-scattering events as the particle penetrates a distance X within the solid. It is usually represented by the multiple-scattering (MS) function $f(\alpha,X)$ which yields the statistical distribution of particles with a total angular deflection α. So we can express the electronic multiple-scattering (EMS) function in the form $F(\alpha,X)d\Omega=f(\alpha,X)d\Omega/2\pi$, where $f(\alpha,X)$ is given in the small-angle approximation by [15]

$$f(\alpha,X)=\int_0^\infty\kappa d\kappa J_0(\kappa\alpha)\exp^{-n_eX\sigma_0(\kappa)}.\qquad(12)$$

The function $\sigma_0(\kappa)$ is determined from the previously defined scattering function $G_{\forall T}(q_\perp)$, for the present case of a PDEF, which takes the form

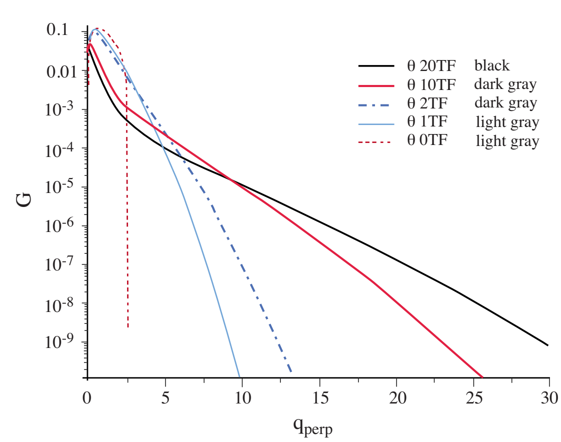

FIG. 5. (Color online) Same caption as Fig. 3 with enlarged q_{perp} range.

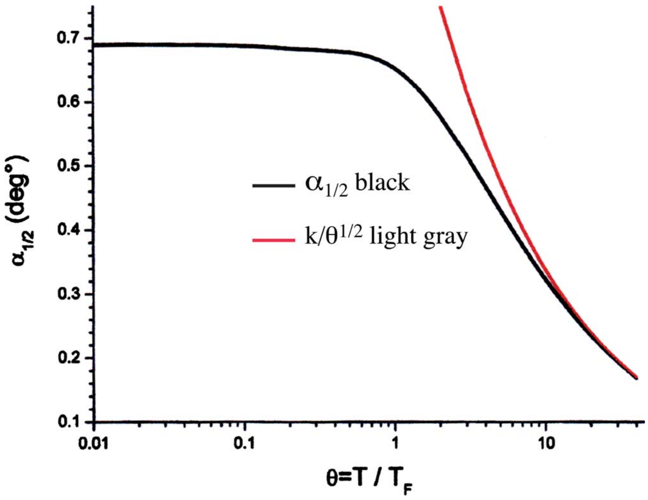

FIG. 6. (Color online) $\alpha_{1/2}$ (in degrees) in terms of T/T_F in an electron target with density r_s=1.5 and thickness X=800 a.u. (0.0424 μm). $k \approx 1$.

$$\sigma_{0\forall T}(\kappa) = \int [1 - J_0(\kappa\psi)]d\sigma$$

$$= \frac{1}{n_e}\int_0^\infty \left[1 - J_0\left(\frac{\kappa q_\perp \hbar}{M_1 v_p}\right)\right] G_{\forall T}(q_\perp) dq_\perp, \quad (13)$$

with $q_\perp$ qualifying a classical and nondegenerate upper bound. In this connection, it is worthwhile to notice that replacing the given infinite upper limit by the fully degenerate $2q_F$ one does not change significantly the $\sigma_0(\kappa)$ estimate. Finally, we reach the angular distribution function explained at Eq. (12) for a given penetration depth X in target.

B. Half width at half maximum angle $\alpha_{1/2}$

Analysis of quadrature of the previously reached Eq. (12) essentially relies on $\alpha_{1/2}$, the half angle at half maximum, fulfilling $f(\alpha,X)=f(0,X)/2$. The usefulness of this concept is successively highlighted through its T dependence, X dependence, v_p dependence, as well as n_e (or r_s) dependence.

The T dependence is documented on Fig. 6 as a monotonous decay for a PDEF target $\theta \geq 1$ with $n_e \approx 4.8 \times 10^{23}$ and a thickness X=0.0424 μm (800 a.u.), while the strongly degenerate regime ($\theta < 1$) features a nearly horizontal plateau. At every θ value, the thickness dependence follows the Gaussian-like trend

$$\alpha_{1/2} \propto \sqrt{X} \quad (14)$$

already featured at θ=0 [6].

V. BEYOND THE BETHE APPROXIMATION

Usually, the right-hand side of Eq. (13) is estimated through the assumption (M_1, ion projectile mass)

$$\frac{\kappa_{q_\perp}}{M_1 V_p} \ll 1, \quad (15)$$

with the Bethe ansatz [17]

$$1 - J_0\left(\frac{\kappa_{q_\perp}}{M_1 v_p}\right) \cong 1/4\left(\frac{\kappa_{q_\perp}}{M_1 v_p}\right)^2, \quad (16)$$

which we intend to enlarge here. Usually, one assumes that for heavy ions with $M_1 \ggg m_e$ at nonzero v_p, this ansatz is a robust one. However, if one has to consider lighter projectiles such as mesons or electrons and arbitrary small projectile velocities as well, one might encounter difficulties, even if the $\kappa \to \infty$ limit is handsomely taken into account by a sufficiently fast decaying κ integrand, while the above computed $G(q_\perp)$ also decreases faster than $\bar{q}_\perp^4$ as $q_\perp \to \infty$.

A typical quantity of interest, the mean-free path (mfp) l, thus writes as (in a.u.)

$$\frac{1}{\ell} = \frac{1}{4}\frac{\kappa^2}{(M_1 v_p)^2}\bar{q}_\perp^2 = \frac{1}{4}\kappa^2\bar{\psi}^2, \quad (17)$$

where

$$\bar{q}_\perp^2 = \int_0^\infty q_\perp^2 G(q_\perp) dq_\perp \quad (18)$$

and

$$\bar{\psi}^2 = \frac{\bar{q}_\perp^2}{(M_1 v_p)^2}, \quad (19)$$

when one restricts to the Bethe ansatz (16).

Now, we propose to relax the constraint (15) with the finite and alternate series [18]

$$1 - J_0(x) = 4\left(\frac{x}{4}\right)^2 - 4\left(\frac{x}{4}\right)^4 + 1.777\,756\left(\frac{x}{4}\right)^6 - 0.444\,358\,4\left(\frac{x}{4}\right)^8 + 0.070\,925\,3\left(\frac{x}{4}\right)^{10} - 0.007\,672\,2\left(\frac{x}{4}\right)^{12} + 0.000\,501\,441\,5\left(\frac{x}{4}\right)^{14} + \varepsilon_0(x), \quad (20)$$

with $|\varepsilon_0(x)| \leq 10^{-9}$ for $-4 \leq x \leq 4$, which extends the Bethe ansatz (16) and expression (17) for $1/\ell$ to

$$\frac{1}{\ell} \cong \frac{\bar{\psi}^2}{4}\bar{q}_\perp^2 - \frac{\bar{\psi}^4}{4^3}\bar{q}_\perp^4 + 1.777\,756\frac{\bar{\psi}^6}{4^6}\bar{q}_\perp^6 - 0.444\,358\,4\frac{\bar{\psi}^8}{4^8}\bar{q}_\perp^8 + 0.070\,925\,3\frac{\bar{\psi}^{10}}{4^{10}}\bar{q}_\perp^{10} - 0.007\,672\,2\frac{\bar{\psi}^{12}}{4^{12}}\bar{q}_\perp^{12} + 0.000\,501\,441\,5\frac{\bar{\psi}^{14}}{4^{14}}\bar{q}_\perp^{14}, \quad (21)$$

where

$$\bar{q}_\perp^{2p} = \int_0^\infty q_\perp^{2p} G_{\forall T}(q_\perp) dq_\perp. \quad (22)$$

By inspecting Figs. 3–5, it is obvious that the $2p$ momenta (22) remain finite. However, they can reach very high values for p=6 or 7, which can severely restrict the $\bar{\psi}$-validity range. Nonetheless, the extension (20) proves useful at not

TABLE I. $\bar{\psi}$ [Eq. (19)] and R [Eq. (28)] in terms of T_F for $T/T_F=1$.

$T_F=0.29$ $N_e=10^{23}$ cm^{-3}		$T_F=1.34$ $N_e=10^{24}$ cm^{-3}		$T_F=6.215$ $N_e=10^{25}$ cm^{-3}		$T_F=28.85$ $N_e=10^{26}$ cm^{-3}	
$\bar{\psi}$	R	$\bar{\psi}$	R	$\bar{\psi}$	R	$\bar{\psi}$	R
0.01	0	0.01	0	0.01	0	0.01	0
0.05	0	0.05	0	0.05	0	0.05	0.02
0.1	0	0.1	0	0.1	0	0.1	0.07
0.5	0.026	0.5	0.1	0.5	1.8	0.5	10.6
1.0	0.1	1.0	0.3	1.0	4.2	1	77154
2.0	0.3	2.0	6.34	2.0	26086		
3.0	0.48						
4.0	0.54						

high a temperature ($T\leq 3\ T_F$), while it allows converging alternate series (21) up to $\bar{\psi}\cong 1$, which already enlarges considerably the validity domain of the initial Bethe ansatz (16).

A deeper insight is also afforded by a direct and analytic estimate of Eq. (22) with Eq. (10) in atomic units, so that (p€ [1–7])

$$\bar{q}_{\perp}^{2p}=\frac{2Z^2}{\pi}\frac{(8T)^{p-1/Z}}{(p+1)}\int_{q_\perp}^{\infty}\frac{u^{(2p+Z)}du}{(u^2+u_s^2)^2(1+e^{u^2-\eta})} \tag{23}$$

after integrating by parts, where (T in a.u.)

$$u^2=\frac{q^2}{8T}\quad\text{and}\quad u_S^2=\frac{q_S^2}{8T}.$$

Expression (23) is further explained through

$$u_S^2=\frac{q_{\mathrm{TF}}^2}{16T}\left(\frac{T}{T_F}\right)^{1/2}F-\frac{1}{2}(\eta), \tag{23a}$$

with

$$q_{\mathrm{TF}}^2=3\left(\frac{T_F}{1.84}\right)^{3/2}\frac{1}{\left(T^2+\frac{4}{9}T_F^2\right)^{1/2}} \tag{24}$$

and [8]

$$F_{-1/2}(\eta)\cong\frac{4}{(4\theta+9\theta^3)^{1/2}},\quad \theta=\frac{T}{T_F}. \tag{25}$$

A more precise albeit involved Padé approximation for $F_{-1/2}(\eta)$ may alternatively be used [9]. On the other hand, one can also introduce

$$\eta=\frac{\mu^0(T)}{T}, \tag{26}$$

where $\mu^0(T)$ and T are in T_F, with [19] and

$$\mu^0(T)=\exp\left[-\frac{t^2}{12}+A_1t^2\right]+2.718\mu>(T)\exp(-1-A_2t^{-2}-A_3t^{-4}), \tag{27a}$$

with

$$t=\pi T,\quad A_1=0.178,\quad A_2=1,75,\quad A_3=59.4,$$

while

$$\frac{\mu^>}{T}=-\ln(6\pi^2)+1.5\ln\frac{4\pi}{T}+\cdots. \tag{27b}$$

A first test of the above derivation is performed with $T/T_F=1$ and $T_F=3$ in a.u, which in the fast ignition scenario (FIS) for inertial confinement fusion (ICF) [16] yields 0.0475 for the first term in the right-hand side of Eq. (21) with $\bar{\psi}=1$, although the whole series amounts to 0.0429. On the other hand, at FIS ignition ($T/T_F=1$) with $n_e\cong 10^{26}$ e cm^{-3} ($T_F\cong 29$), the series (21) converges only with $\bar{\psi}=0.1$ to its first

TABLE II. Same caption as Table I for $T/T_F=0.1$ and $T_F=28.85$.

$\bar{\psi}$	R
0.01	0
0.05	0.002
0.1	0.007
0.5	0.58
1	19

TABLE III. Same caption as Table II for $T_F=0.3$.

$\bar{\psi}$	R
1	0.0045
2	0.21
3	0.40
4	0.58

term which nevertheless significantly improves on the extreme inequality (15).

A wider perspective is offered in Table I at $T/T_F=1$ and for target electron densities of FIS concern, i.e., $10^{23} \leq N_e$ (cm^{-3})$\leq 10^{26}$, with $0.29 \leq T_F \leq 28.85$. Then, we consider the ratio

$$R = \left| \frac{\frac{\bar{\psi}^2 \bar{q}_\perp^2}{4} - [\text{RHS Eq. (21)}]}{\frac{\bar{\psi}^2 q_\perp^2}{4}} \right| \tag{28}$$

in terms of $\bar{\psi}$ [Eq. (19)]. Table I shows that for $\bar{\psi} \leq 0.1$, the restriction to the first term in Eq. (21) remains an excellent approximation for any T_F value. It persists as a possible one up to $\bar{\psi}=1$ for $T_F=0.3$ and 1.34. Above $\bar{\psi}=1$ and for higher T_F values, the ratio R can demonstrate an explosive increase, invalidating completely the so-called Bethe ansatz.

Corresponding physical situations primarily highlight multiple scattering of lighter projectiles such as electrons and mesons in a strongly degenerate electron target. Switching attention to strongly degenerate electron targets featuring $T/T_F=0.1$, one witnesses contrasting robustness behaviors of very dense (Table II) and moderately dense targets (Table III). In the first case, R remains close to zero only with $\bar{\psi} \leq 0.1$, while in the second case, one sees that $\bar{\psi} \leq 1$ fulfills this requirement.

It should be appreciated that $T/T_F=0.01$ would produce nearly identical outputs. On the other hand, in the high-temperature range $T/T_F \geq 1$, the robustness of the Bethe ansatz decreases with increasing T as evidenced on Table IV.

TABLE IV. R values [Eq. (28)] for $T_F=0.3$ in terms of T/T_F.

T/T_F / $\bar{\psi}$	1	4	10	100
0.01	0	0	0	0
0.05	0	0	0	0.012
0.1	0	0	0.005	0.047
0.5	0.026	0.054	0.11	6.54
1	0.1	0.18	0.3	47700.4
2	0.3	0.0005	156	
3	0.48	91.4		
4	0.54			

VI. SUMMARY

We have extended to any temperature a former $T=0$ [6] FEG multiple-scattering formalism for a low velocity ($v_p < v_{\text{the}}$) ion projectile stopped in a PDEF of potential WMD concern. The relevant $\alpha_{1/2}$ parameter exhibits a significant temperature dependence.

These calculations are of relevance to deuterium-tritium targets with $n_e \geq 10^{24}-10^{26}$ cm^{-3} at $T\varepsilon[0.5;2]$ keV submitted to proton beams in the MeV energy range in order to achieve fast ignition in ICF [16]. They also pave the way to extending multiple-scattering studies to projectiles with any mass, not only heavy ions, as far as arbitrary degenerate electron targets are considered.

ACKNOWLEDGMENT

Part of this work has been supported by the Euratom-CEA Contract No. 3599.001.

[1] C. Deutsch and R. Popoff, Laser Part. Beams **24**, 421 (2006).
[2] B. G. Logan *et al.*, Nucl. Fusion **45**, 131 (2005).
[3] L. Grisham, Phys. Plasmas **11**, 5727 (2004).
[4] K. Morawetz and G. Röpke, Phys. Rev. E **54**, 4134 (1996).
[5] A. A. Solodov and R. Betti, Phys. Plasmas **15**, 042707 (2008).
[6] C. D. Archubi and N. R. Arista, Phys. Rev. A **72**, 062712 (2005).
[7] C. Gouedard and C. Deutsch, J. Math. Phys. **19**, 32 (1978).
[8] N. R. Arista and W. Brandt, Phys. Rev. A **29**, 1471 (1984).
[9] R. G. Dandrea, N. W. Brandt, and A. E. Carlsson, Phys. Rev. B **34**, 2097 (1986).
[10] J. Lindhard, Mat. Fys. Medd. K. Dan. Vidensk. Selsk. **28**, 1 (1954).
[11] B. D. Fried and S. D. Conte, *The Plasma Dispersion Function* (Academic, New York, 1961).
[12] G. Maynard and C. Deutsch, Phys. Rev. A **26**, 665 (1982); **27**, 574 (1983).
[13] I. Nagy, A. Arnau, P. M. Echenique, and K. Ladanyi, Phys. Rev. A **43**, 6038 (1991).
[14] H. R. Ritchie, Phys. Rev. **114**, 644 (1959).
[15] P. Sigmund and K. B. Winterbon, Nucl. Instrum. Methods **119**, 541 (1974).
[16] C. Deutsch, Laser Part. Beams **21**, 33 (2003); Ann. Phys. (Paris) **11**, 1 (1986)
[17] H. A. Bethe, Phys. Rev. **89**, 1256 (1953).
[18] Y. L. Luke, *Integrals of Bessel Functions* (McGraw-Hill Book Co., Inc., New York, 1962), p. 34.
[19] M. W. C. Dharma-Wardana and R. Taylor, J. Phys. C **14**, 629 (1981).